12-1-2021

Photoacoustic-guided endovenous laser ablation: Characterization and in vivo canine study

Yan Yan

Samuel John

Tanyeem Shaik

Bijal Patel

Mai T. Lam

See next page for additional authors

Authors

Yan Yan, Samuel John, Tanyeem Shaik, Bijal Patel, Mai T. Lam, Loay S. Kabbani, and Mohammad Mehrmohammadi
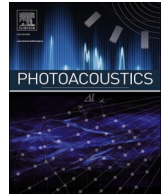
Photoacoustic-guided endovenous laser ablation: Characterization and *in vivo* canine study

Yan Yan [a],[1], Samuel John [a],[1], Tanyeem Shaik [a], Bijal Patel [a], Mai T. Lam [a], Loay Kabbani [b], Mohammad Mehrmohammadi [a],[c],*

[a] *Biomedical Engineering, Wayne State University, Detroit, MI, United States*
[b] *Vascular Surgery, Henry Ford Health System, MI, United States*
[c] *Barbara Ann Karmanos Cancer Institute, MI, United States*

ARTICLE INFO

ABSTRACT

Endovenous laser ablation (EVLA) is a minimally invasive surgical procedure, often guided by ultrasound (US) imaging, for treating venous insufficiencies. US imaging limitations in accurately visualizing the catheter and the lack of a temperature monitoring system can lead to sub-optimal outcomes. An integrated photoacoustic (PA)-guided EVLA system has been previously developed and reported to overcome the shortcomings of US-guided procedure. In this study, we further characterized the system and tested the *in vivo* utility. In addition, PA thermometry was further explored by compensating the variation of PA signal with temperature with respect to the temperature-dependent absorption of blood and water. *In vivo* imaging results indicated that the PA-guided EVLA system can provide high contrast and accurate images of the ablation catheter tip overlaid on US images of the background tissue. Additionally, absorption-compensated PA signal amplitudes over a relevant range of temperature were measured and demonstrated.

1. Introduction

In the United States, chronic venous insufficiencies (CVI) affect approximately 23 % of the adult population at some point in their lifetime [1]. Varicose veins are a manifestation of CVI characterized by the superficial bulging of veins due to the accumulation of blood caused by weakened vein valves [2]. Varicose veins occur in the superficial veins of the lower limbs and rarely in the upper extremities. Untreated CVI can lead to lower extremity edema, venous stasis, dermatitis, and venous ulcers [3,4]. With more than 40 million people in the United States have received some form of treatment for varicose vein diseases, treatment costs are estimated to reach $1 billion annually [5]. Minimally invasive procedures including endovenous laser ablation (EVLA) [6], endoscopic radiofrequency ablation [7], trans-illuminated phlebectomy [8], liquid or foam sclerotherapy [9], and cyanoacrylate adhesives [10] are used for treating varicose veins. EVLA is the most preferred treatment procedure due to the high technical success rate, short recovery time, and minimal post-operative pain [11–13]. EVLA is often guided by ultrasound (US) imaging to assure proper placement of the ablation catheter

within the diseased vein. The localized heat generated at the ablation catheter tip seals the diseased vein. The efficacy of the EVLA procedure depends on the precise placement of the ablation catheter within the vein and limiting the damage to perivenous tissues during ablation. However, the US imaging artifacts such as reverberation [14], and comet tail [15], in addition to its limited contrast and signal-to-noise ratio, limit the ability of US imaging to track the ablation catheter tip within the diseased vein accurately. US imaging loses the ablation catheter tip in angled veins because the US waves reflected from the angled catheter move away from the US imaging plane [16–18]. Improper transducer-catheter alignment and sonographer errors cause tracking-related inaccuracies [19]. US images of the ablation catheter within the surrounding tissues have a poor signal-to-noise ratio (SNR) and contrast-to-noise ratio (CNR), making it difficult to detect the ablation catheter tip within the background tissue. Besides, US imaging is unable to distinguish between the body and the tip of the ablation catheter due to their similar acoustic features. These inaccuracies lead to the cauterization at the incorrect location (near the junction of femoral or the popliteal vein), which may cause deep vein thrombosis (DVT),

---

* Corresponding author at: Biomedical Engineering, Wayne State University, Detroit, MI, United States.
E-mail address: mehr@wayne.edu (M. Mehrmohammadi).
[1] Equal contribution.

and increase the risk of varicose veins recurrence. During vein ablation, a temperature feedback system can provide a non-invasive means to determine the real-time thermal dose deposition and monitor the lesion formation (which leads to vein closure). Some endovenous radio-frequency (RF) ablation systems are equipped with a temperature monitoring system, which prevents the overheating and charring of the tissue [20]. However, the lack of real-time temperature monitoring in EVLA systems may lead to an excessive thermal dose, which causes perivenous damage, hyperemia, ecchymosis [11,21], edema, and endovenous heat-induced thrombosis (EHIT) (1–2 %) [22,23]. An Insufficient thermal dose may cause recanalization and the recurrence of varicose veins (1–20 %). These limitations prolong the duration of the surgery and lead to post complications.

These unmet clinical needs call the need for developing a clinically translatable, low-cost, point-of-care system, which can accurately track the ablation catheter tip and provide real-time temperature monitoring at its tip within the vein. We envision that catheter tip tracking and temperature monitoring capabilities will be improved by integrating photoacoustic (PA) imaging modality into the current EVLA system. PA imaging acoustically probes the thermoelastic responses of the excited optical absorbers through short-pulsed laser illumination [24–26]. US-guided EVLA procedure guides an ablation catheter into the diseased vein. A pulsed laser source can be integrated into the same ablation catheter, adding PA imaging to the existing EVLA system. Our previous ex vivo studies [17] demonstrated a novel PA-guided EVLA system and its characterization results [19] in *ex vivo* phantom and tissue studies. The results indicated that the PA imaging improved the accuracy in tracking the ablation catheter tip since the PA signal is generated only at the interface between the ablation catheter tip and the surrounding medium. The omnidirectional nature of the PA signal enables angle-independent ablation catheter tip tracking. Several research groups have utilized PA imaging for guiding medical procedures that require the placement and positioning of external objects such as metallic needles [27,28], catheters [29], and balloon catheters [30]. Most of these reported methods are using external illumination to perform PA imaging. PA-guided procedures using internal illumination have been reported in robot-guided catheter tracking systems [31,32] and have been used for tracking catheters [29,33]. Additionally, the amplitude of the PA signal is a function of the surrounding temperature. Therefore, PA imaging is an ideal solution for monitoring the real-time temperature in EVLA procedures. PA imaging with external illumination [34,35] has been used for monitoring the real-time temperature and formation of thermal lesions. However, since the PA signal highly depends on the fluence at the temperature monitoring site, external illumination requires an accurate light diffusion model to estimate the fluence and provides reliable and quantitative temperature measurements. In this study, we explored the capabilities of the developed PA-guided EVLA system *in vivo* animal studies. We modified the system's imaging sequence, which makes it is easier to use during the operation. The variation in the PA signal at different imaging depths and orientation angles was characterized. A temperature detection method was developed by calculating the PA signal amplitudes as well as the optical properties of blood and water within the temperature range of 30 °C to 85 °C. Combining these two methodologies, we demonstrated the possibility of performing accurate quantitative PA thermometry, independent from the variation of optical absorption of the blood and water. In the end, we reported the in-vivo PA-guided EVLA procedure imaging results for ablation catheter tip tracking and real-time measurements of the ablation catheter tip temperature. The *in-vivo* experimental results demonstrated the PA-guided EVLA system, and its procedures offers an advantage over the US-guided method and can be potentially translated into the clinic with minimal modifications in the existing EVLA devices.

2. Materials and methods

2.1. Principle of PA thermometry

PA imaging is a hybrid imaging modality that marries optical illumination and US imaging to probe the optical properties of the tissue of interest. The general waveform of a PA signal (P) in a homogeneous inviscid medium at initial temperature T_0 associated with the acoustic attention of the medium can be defined by:

$$P(T_0) \propto \Gamma(T_0)\mu_a(T_0)Fe^{-\alpha_{T_0}d}, \tag{1}$$

During thermotherapy, the difference between detected PA amplitudes when the temperature of the tissue rises from the initial temperature T_0 to T_1 and can be represented as (2):

$$\Delta P(T_0, T_1) \propto P(T_0) - P(T_1), \tag{2}$$

where Γ is the Grüneisen parameter representing the thermoelastic efficiency of the medium; μ_a refers to the absorption coefficient of the chromophore. F is denoted as the laser fluence; d refers to the distance that the acoustic waves traveled between the acoustic source (imaged ablation catheter tip) and the transducer; and α_{T_0} represents the acoustic attenuation coefficient along the direction of d at the temperature T_i.

By solving Eq. (2) with the fluence measurements, optical properties, Grüneisen parameter, and acoustic attenuation of the medium, accurate quantitative thermometry can be performed. However, the quantitative temperature estimation in the developed PA-guided EVLA system is relatively easy since most of the terms, including fluence and acoustic attenuation of the tissue medium, are negligible. During EVLA procedures, the distance between the ablation catheter and the transducer is relatively constant. Moreover, the heat and PA signal generated at the ablation catheter tip is localized, occurs internally, and does not cause a significant rise in temperature in the tissue medium. Hence, minimal acoustic attenuation changes occur at the tissue medium between the transducer and the ablation catheter. Thus, the changes in the acoustic attenuation coefficient are very minimal. Moreover, the fluence F is a constant because the pulsed laser illumination does not penetrate the tissue layers. Therefore, by removing the attenuation term and using a constant fluence in the initial PA signal generated at the ablation catheter tip, (2) can be rewritten as:

$$\Delta P(T_0, T_1) \propto \Gamma(T_0)\mu_a(T_0) - \Gamma(T_1)\mu_a(T_1), \tag{3}$$

From the literature, the tissue parameters, such as absorption properties for blood, have been reported to increase from 25 °C to 55 °C [36]. However, at higher temperatures above 55 °C, the optical properties of blood changes due to protein denaturation [37]. Therefore, by measuring temperature-dependent variations in the medium's optical properties, it is possible to find a direct relation between PA signal change and variations of the Grüneisen parameter and, thus, perform accurate and quantitative thermometry during the PA-guided EVLA procedure. The quantitative relationship of temperature with absorption compensated PA amplitude can be calculated as:

$$\Delta T \propto \Delta \Gamma(T_0, T_1) = \frac{\Delta P(T_0, T_1)}{\Delta \mu(T_0, T_1)} \tag{4}$$

2.2. Integrated PA-guided EVLA system

The PA-guided EVLA system integrated a beam merging system and a USPA imaging system. The beam merging system combined the beams from a single wavelength (532 nm), 10−28 Hz pulsed laser (LumiBird, Montana, USA), and a clinical continuous-wave (CW) ablation laser (Venacure 1470, wavelength λ = 1470 nm, Angiodynamics, New York, USA) into an ablation catheter. Fig. 1**a** shows a photograph of the beam merging system, and Fig. 1**b** shows the principle of merging two laser beams. By using a cold mirror (CMR 45, Newport, Irvine, CA, USA), the
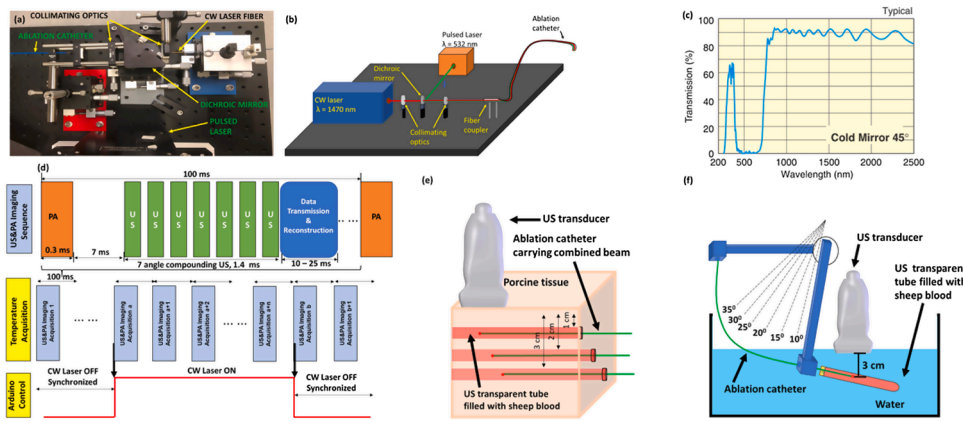
Fig. 1. (a) Photograph and (b) Schematic diagram of the of the PA-guided EVLA system. The pulsed laser beam from the pulsed laser and the CW laser beam from the CW laser is combined using cold mirror into a single ablation catheter through collimation optics. (c) The cold mirror has a higher transmission at wavelengths ranging from 780 nm to 2500 nm and high reflectance of wavelengths ranging from 400 nm to 700 nm. Image adapted from Newport. (d) Timing diagram indicating the US&PA imaging sequence and temperature monitoring synchronization with US & PA image acquisition and ablation. Schematic of the experimental setup (e) to evaluate the change in PA amplitude at different depths within a porcine tissue at different pulse energies, and (f) to measure the PA amplitude within a blood medium at different catheter orientations.

laser beams can be merged and coupled into an ablation catheter (FP1000ERT, core diameter 1000 μm, numerical aperture 0.5, Thorlabs, New Jersey, USA) by a set of collimating lenses (LB1761, LA1116, Thorlabs, New Jersey, USA). The optical properties of the mirror are shown in Fig. 1c. The maximum power of the CW laser is 10 W. The total energy loss for the CW laser is about 20 % due to optics, which is sufficient for the EVLA procedure.

The imaging component of the PA-guided EVLA system comprised of a high-frequency linear array US transducer (L11−4v, 128 elements, bandwidth 4−11 MHz, Verasonics, Washington, USA), equipped with a digital US research platform (Vantage 128, Verasonics, Washington, USA). A function generator (RIGOL Technologies, Beijing, China) was used to synchronize the pulsed laser system and the imaging system to confirm the accuracy of the real-time co-registered USPA images. A microcontroller in coordination with the function generator was used to synchronize the CW laser and the pulsed laser. The imaging sequences were shown in Fig. 1d.

2.3. Ex vivo characterization of EVLA-guided system to evaluate the maximum imaging depth and minimum required pulsed energy

The PA-guided EVLA system utilizes an internal illumination light delivery system, in which a constant fluence is maintained. Hence, the PA signal flight through the tissue layers is affected by acoustic attenuation. We performed a study to characterize the acoustic attenuation of PA signals at different imaging depths. These studies were performed by placing the ablation catheter carrying the combined beam (λ = 532 nm and λ = 1470 nm) into US transparent tubes (diameter 0.5 cm, Zeus, South Carolina, USA) filled with heparinized sheep blood (Cedarlane, Canada). The tubes were then embedded at different depths (1, 2, 3 cm) within a porcine tissue (Fig. 1e). The depths were selected based on the common locations of EVLA based varicose vein treatment procedures. The PA amplitude was acquired at each depth with a sagittal view of the ablation catheter tip at different pulse energies (50, 100, 150 μJ), respectively. These measurements also include the effect of acoustic attenuation on the PA signal generated at each depth. Moreover, this experiment aims to determine the minimum pulse energy required for the system while imaging deep tissues. Additionally, we designed the following orientation-depth experiments to validate that the PA signal is independent of the ablation catheter orientation at a constant imaging depth (Fig. 1f). In the experiments, the same ablation catheter and US transparent tube described above were used. Instead of placing the tubes at different depths, the tubes were placed within a water medium at a constant depth of 3 cm at different orientation angles. Sagittal USPA images of the ablation catheter tip were acquired. The orientation angles were varied from 10 ° to 35 ° at intervals of 5 °. The pulse energy carried by the ablation catheter was varied (50, 100, 150 μJ). By combining the

results of these two experiments, the optimal fluence for *in vivo* studies can be determined.

2.4. Measurement of temperature-dependent optical absorption of blood and water

EVLA procedures utilize a high-power CW laser for ablation procedures and induce high-temperature changes within the vein. At higher temperatures exceeding 55 °C, blood denatures, coagulates, and the optical absorption properties are altered [37]. These variations in the optical absorption properties affect the PA signal. Previous studies indicated that the absorption coefficient of blood increases in the lower temperature range from 10 °C to 55 °C [36]. To measure the absorption properties of blood in the higher temperature range from 55 °C to 85 °C, we designed an experiment involving a) heparinized canine blood and b) distilled (DI) water whose temperature was varied between 30 °C to 85 °C. Recently developed endovenous laser ablation procedures are often aimed at water-based venous tissues for heating and sealing the veins. In other words, these lasers are tuned to peak absorption of water (1470 nm) to generate thermal lesions [6,38]. Hence, DI water was also included in the study to study the behavior of the absorption changes of water at higher temperatures. The optical absorption properties were studied by suspending a cuvette (path length: 10 mm, Hellma Analytics, New York, USA) filled with heparinized canine blood diluted with phosphate-buffered saline (PBS) at a 1:500 ratio. The cuvette was then heated in a homogenous fashion by a water bath (Fig. 2, **supplementary document**). A K-type thermocouple (Reed Instruments, North Carolina, USA) connected to a microcontroller was used to record the blood temperature at time intervals of 0.5 s. The absorbance of the canine blood was calculated by measuring the incident and transmitted pulsed laser energy (λ = 532 nm) by the Beer-Lambert law [39]. The incident and transmitted energies were recorded by a power meter (PE50BF-- DIFH-C, Ophir Optronics, Utah, USA).

2.5. PA thermometry and lesion formation capabilities of the PA-guided EVLA system

The PA-guided EVLA system provides simultaneous catheter tip tracking, ablation, and real-time temperature monitoring feedback. The capability of the PA thermometry was characterized by acquiring the PA signals of canine blood and water at different temperatures ranging from 30 to 85 °C. An ablation catheter carrying a pulsed laser beam (wavelength λ = 532 nm, energy of 100 μJ) was placed within the same US transparent tube separately filled with a) heparinized canine blood, and b) DI water. The samples were heated up by a water bath. The medium was selected based on the possible imaging conditions during EVLA procedures, (a) the tip of the ablation catheter can be placed close to the
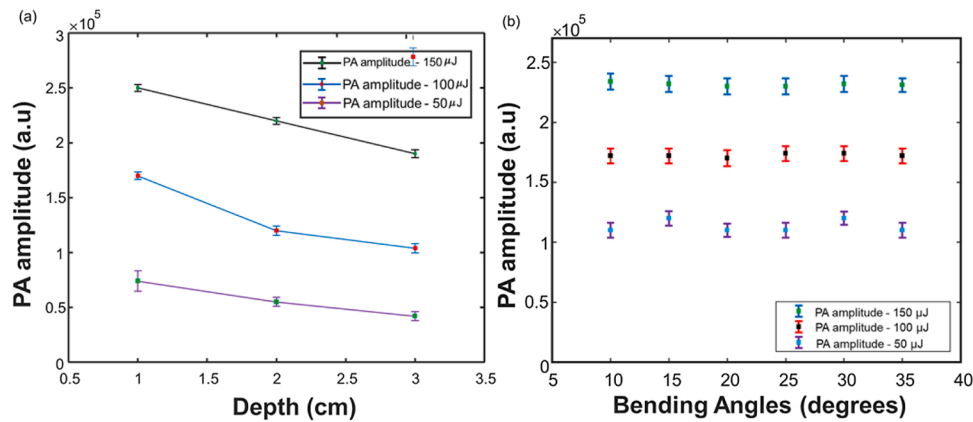
Fig. 2. (a) Variation of PA amplitude at different laser energies, placed at different depths inside the blood tubes, embedded within the porcine tissue. (b) Variation of the PA amplitude at different, different pulse laser energies, placed at different angles inside a blood tube held within a water medium at a constant depth of 3 cm. The error bars represent the standard deviation along each measurement.

inner vein wall (whitish, water-based tissue), or (b) the ablation catheter is suspended inside the lumen at a suitable distance from the vein wall (emerged in the blood). The same K-type thermocouple was placed near the ablation catheter tip to measure the temperature of the medium during the study. A Polyvinyl chloride (PVC) phantom was used as the coupling medium to prevent direct contact between the US transducer and the hot water within the container. Sagittal US and PA images of the ablation catheter were acquired. Attenuation caused by the PVC due to temperature variations was compensated. The PA amplitude was computed by averaging the PA signals at the ablation catheter tip. These measurements were repeated three times to analyze the robustness of the measurements. The boundary of the tube or the tube wall will not influence the PA signal since the illumination at the catheter tip is a point illumination and illuminates a very small distance in front of the catheter tip. The PA signal generated is always seen within a homogenous medium and is not affected by the discontinuities in water.

The lesion formation capabilities of the PA-guided EVLA system were also evaluated through *ex vivo* experiments. Since the CW laser in the integrated system passes through a series of optics before exiting the ablation catheter, analyzing this parameter is critical in the developed system. In this experiment, the ablation catheter carrying the combined beam ($\lambda = 532$ nm, 200 µJ, and $\lambda = 1470$ nm, 8 W) was placed inside the excised jugular vein of a canine model (length = 10.5 cm, diameter = 0.5 cm). The temperature sensor was placed on the outer vein wall in a perpendicular arrangement to the ablation catheter. A gelatin block was placed on top of the vein to enable imaging of the vein. The ablation laser remained active for 2.5 s during the procedure. US and PA images were recorded before and after the period of the ablation procedure. Studies were performed *ex vivo* to have better control on the ablation site and perform the histological analysis on the ablated site with better accuracy. Hematoxylin and Eosin (H&E) were used for staining the ablated and non-ablated regions of the vein tissue sections to indicate that the vein was successfully ablated. The ablated vein was cut into two pieces, and the ablated site was marked based on the discoloration and changes in the PA signal. The distance between the ablated and non-ablated sites was roughly measured as 1 cm. Both tissue regions were excised from the vein and fixed in formalin for 24 h. Then they were dehydrated in increasing ethanol changes from 70 % to 100 % over 8 h, cleared in xylenes for 2 h, and embedded in paraffin. The embedded tissues were sectioned at 8 µm thickness for staining.

2.6. In vivo ablation catheter tip tracking in a canine model

The capabilities of PA imaging to track the ablation catheter was evaluated by placing an ablation catheter carrying the combined beam ($\lambda = 532$ nm, 200 µJ, and $\lambda = 1470$ nm, off) into the jugular vein of a dog

(Fig. 1a, **supplementary document**). Two dogs were used for the study. The canine study protocol and the animal handling were approved by the Institutional Animal and Care Use Committee of Henry Ford Health Systems. A US gel block was used on the scanning region (Fig. 1b-c, **supplementary document**) to ensure acoustic coupling between the US transducer and the skin. Transverse and Sagittal USPA images of the ablation catheter tip within the vein were acquired (Fig. 1d, **supplementary document**). The SNR and the CNR of the USPA images were calculated. The SNR was defined as:

$$SNR = 20\log_{10}\frac{\mu_{signal}}{\sigma_{background}} \quad (5)$$

where μ_{signal} refers to the mean signal generated at the tip of the ablation catheter, and $\sigma_{background}$ refers to the standard deviation of the background (anatomical structure of the vein). The CNR was calculated as:

$$CNR = 20\log_{10}\frac{|S_{catheter} - S_B|}{\sigma_{background}}, \quad (6)$$

where $S_{catheter}$ refers to the mean of the desired signal (at the tip of the ablation catheter), S_B refers to the mean of the background (anatomical structure of the vein), and $\sigma_{background}$ represents the background noise.

2.7. Evaluating the feasibility of in vivo PA thermometry in a canine model

The ability of PA imaging to perform non-invasive sensing of the real-time temperature inside the vein of a live dog (animal information is the same as studies in 2.6) was evaluated by placing an ablation catheter carrying the combined beam ($\lambda = 532$ nm, 200 µJ, and $\lambda = 1470$ nm, 12 W) and a K-type thermocouple (Fig. 1e, **supplementary document**). Fig. 1e shows the arrangement of the ablation catheter and the temperature sensor. Tumescent anesthesia was injected along the length of the fascia of the jugular vein to lower the temperature and prevent damages to the perivenous tissue. Transverse and sagittal USPA images of the ablation catheter tip within the vein were acquired during ablation. The thermocouple was equipped with a data-logging system developed on a microcontroller platform.

3. Results

3.1. The depth and energy-dependent PA for tracking the catheter tip at different angular orientations

Fig. 2 shows the experimental results for evaluating the PA signal amplitude at different imaging depths and ablation catheter

orientations. The results in Fig. 2a indicated that the system could detect the PA signal generated at the ablation catheter tip at a pulse energy of 50 μJ, placed at an imaging depth of 3 cm. The variations in the PA amplitude at the same depth are due to the change in laser fluence. The acoustic attenuation introduced the variations with the same fluence at a different depth, which is nearly linear and follows the principle of acoustic attenuation. The averaged acoustic attenuation computed is about 0.1 dB/cm, which can be negligible during *in vivo* studies since it is close to the background noise level. Fig. 2b describes the variation in the PA amplitude at different ablation catheter orientations. Unlike US imaging, which loses the ablation catheter tip at an angle of 30 °, the US transducer detects these omnidirectional acoustic waves. Also, in contrast to the attenuation suffered by the PA signals in the porcine tissue, the PA amplitude at constant laser energies suffers minimal attenuation in the water medium. Unlike external illumination, which is affected by fluence absorption by the surrounding tissues, the proposed system uses internal illumination, where the laser fluence is constant. These studies provide the selected range of laser energies, which can be used for ablation catheter tip tracking and monitoring the real-time temperature in animal studies and future clinical trials. The internal illumination-based PA thermometry system will not be affected by varying fluence, imaging depth, and orientation of the ablation catheter within the vein. Hence, our PA thermometry system can be calibrated *ex vivo*. These calibration studies will provide a temperature-dependent PA curve, which can provide quantitative temperature information during animal studies. While most of the results in the characterization studies were acquired when the catheter was static, visualization of the moving catheter is anticipated to produce identical results. Moreover, in our recent study, we have demonstrated the dynamic tracking of the catheter tip with low and high-repetition-rate enabled PA imaging [40].

3.2. Characterization of blood and water absorption properties for absorption-compensated PA thermometry

Fig. 3a shows the change in absorbance of canine blood with temperature. From Beer and Lambert's law [39], the absorbance measurements can be directly related to the absorption coefficient parameter since the measurements were done in cuvettes with a constant and relatively short path length, which minimizes the effect of scattering. In addition, the cuvette had an anti-reflection coating, and therefore, the reflection-related losses were minimized. Consequently, the measured absorbance was dominated by the absorption of the material. The results indicated the absorption of blood slightly increases in the temperature

range from 30 °C to 55 °C. After a temperature of 55 °C, a rapid decrease of absorption was detected until 80 °C, followed by saturation in the absorption from 80 °C up to 85 °C. The variation of absorption in the lower temperature range matches the results reported in the literature [36]. Fig. 3d indicated the absorption of DI-water has a constant increase in the same temperature range as the canine blood. Fig. 3b and Fig. 3e show the detected PA amplitudes for blood and water during a slowly heating-up process. In these measurements, the PA amplitude acquired at various temperatures was normalized to the maximum PA amplitude. The canine blood study revealed a nonlinear variation of the PA amplitudes at higher temperatures. The drop in the PA amplitude at 55 °C matches the decrease in its optical absorption. This drop is due to the denaturation and coagulation of blood, followed by the alteration in its optical properties [37]. It is hypothesized that partial denaturation of blood occurs at (>55 °C), followed by complete denaturation at 65−70 °C. It is assumed that blood experiences a change in phase during this temperature interval. However, the increase in PA amplitude after 70 °C in the normalized results can be accounted for due to the combined effect, including the absorption changes and the Grüneisen parameter. In contrast, the PA amplitude changes of DI-water exhibited a linear change (Fig. 3e) until 80 °C, which was in accordance with the increase in its absorption (Fig. 3d). Moreover, our previous studies [17] have validated the linear relationship of PA amplitude with temperature variations within a DI water medium (until 85 °C) in a closed environment. However, the decrease in PA amplitude can be explained due to the starting of phase changes in water that form bubbles at the ablation catheter tip, which is usually negligible in a closed environment. Fig. 3c and Fig. 3f show the compensated PA thermometry results. The compensated results were computed by normalizing the PA amplitude (Fig. 3b, e) at different temperatures by the changes in the optical absorption of the medium (Fig. 3a, d) measured at the same temperatures as shown in Eq. 7:

$$Compensated\ PA\ amplitude = \frac{Normalized\ PA(T)}{Absorption(T)} \qquad (7)$$

Where *PA(T)* represents the detected PA signal at a temperature of *T* and *absorption(T)* represents the measured absorption of the surrounding matter (water or blood) at the same temperature. In other words, the compensated results show the PA signal, independent from temperature-dependent variations of the optical absorption of the surrounding medium and will be the function of the Grüneisen parameter. The compensated result of DI water indicated a clear linear relationship between PA amplitude and temperature. In contrast, the compensated
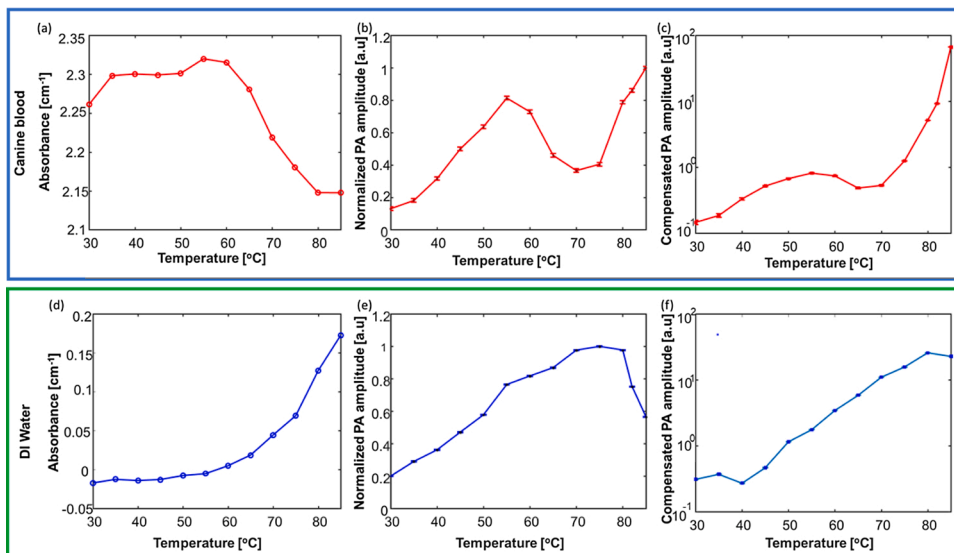

Fig. 3. The top panel highlights the calibration study results of canine blood and the bottom panel indicates the calibration results of DI water. The Variation of absorbance of (a) canine blood and (d) DI water at temperature from 30 °C to 85 °C. Variation of normalized PA amplitude at temperature from 30 °C to 85 °C within (b) canine blood and (e) DI water medium. Compensated PA thermometry measurements at temperature from 30 °C to 85 °C within (c) canine blood and (f) DI water medium. The error bars (b, c, e, f) represent the standard deviation along each measurement.

PA thermometry of canine blood shows an increase in the PA signal amplitude until 55 °C, followed by a drop until 65 °C, and then sharply increases until 85 °C. The increase in the PA signal at temperature (>70 °C) is due to the Grüneisen parameter because the temperature-dependent absorption changes were compensated. This compensated result established a relation between the PA signal and temperature for performing quantitative thermometry.

3.3. Thermal lesion formation using the integrated PA/ EVLA system

The ability of the integrated PA/ EVLA system to form a thermal lesion was evaluated by placing the ablation catheter carrying the combined beam and a miniaturized temperature sensor within an excised vein tissue (Fig. 4a and b). Initially, the PA amplitude increases with the change in temperature at the vein wall (Fig. 4c). The increase in the PA amplitude is due to the alteration of the Grüneisen parameter of tissues. However, the PA amplitude decreases at temperatures ranging from 44 °C to 48 °C due to the thermal lesion formation in the vein wall. In addition, these temperature values correlate with the temperatures causing irreversible cell death, tissue necrosis, which eventually leads to vein closure (Fig. 4b). Histology studies were performed to evaluate the cauterization capability of the CW laser by performing histology studies on the healthy and ablated regions of the venous tissue. The non-ablated region consisted of an intact tunica intima with thin flat endothelial cells and minimal subendothelium. The tunica media appeared thin with smooth muscle layers and connective tissue. The thicker tunica adventitia consisted of abundant collagen and few elastic layers (Fig. 4d). In contrast, the ablated region of the vein tissue (Fig. 4e) indicated extensive coagulative necrosis of smooth muscle in the tunica media region of the vein and partly involving the adventitial layer. The adventitial layer appeared hypereosinophilic (pinkish region indicating

cell damage) with nuclear debris (Fig. 4e, indicated by black arrows). The ablated venous tissue region also revealed prominent degeneration of collagen ablation catheters in the adventitial layer. In conclusion, histology studies indicated a prominent distinction between the healthy and the ablated tissues and demonstrates that the vein is ablated.

3.4. In vivo ablation catheter tip tracking

Fig. 5a-b shows the two transverse and Fig. 5c sagittal co-registered real-time USPA images during the EVLA procedure. The PA images indicated artifact and background-free images, and the US images provide anatomical structures such as the carotid artery in the background. Unlike US imaging, which visualizes the ablation catheter body, PA imaging provides high contrast images of the ablation catheter tip (Fig. 5e). In some cases, transverse US images show no clear distinction between the ablation catheter tip, body, and the background tissue because they share similar US features (Fig. 5d). These limitations cause false readings about the ablation catheter tip location in the vein. However, PA imaging accurately detects the ablation catheter tip inside the vein because the PA signal is generated where the laser pulses emerging from the ablation catheter tip interact with the surrounding blood medium. Based on (5) and (6), the SNR and the CNR of the transverse US image were calculated as 9 dB and 2.1 dB, respectively. The SNR and the CNR of the transverse PA image were calculated as 21.6 dB and 18.2 dB, respectively. The PA images' high SNR and CNR enable easy and accurate detection of the ablation catheter tip. Hence, these overlaid USPA images will provide easy detection of the ablation catheter tip, significantly reducing the surgery duration and minimizing complications in patients.
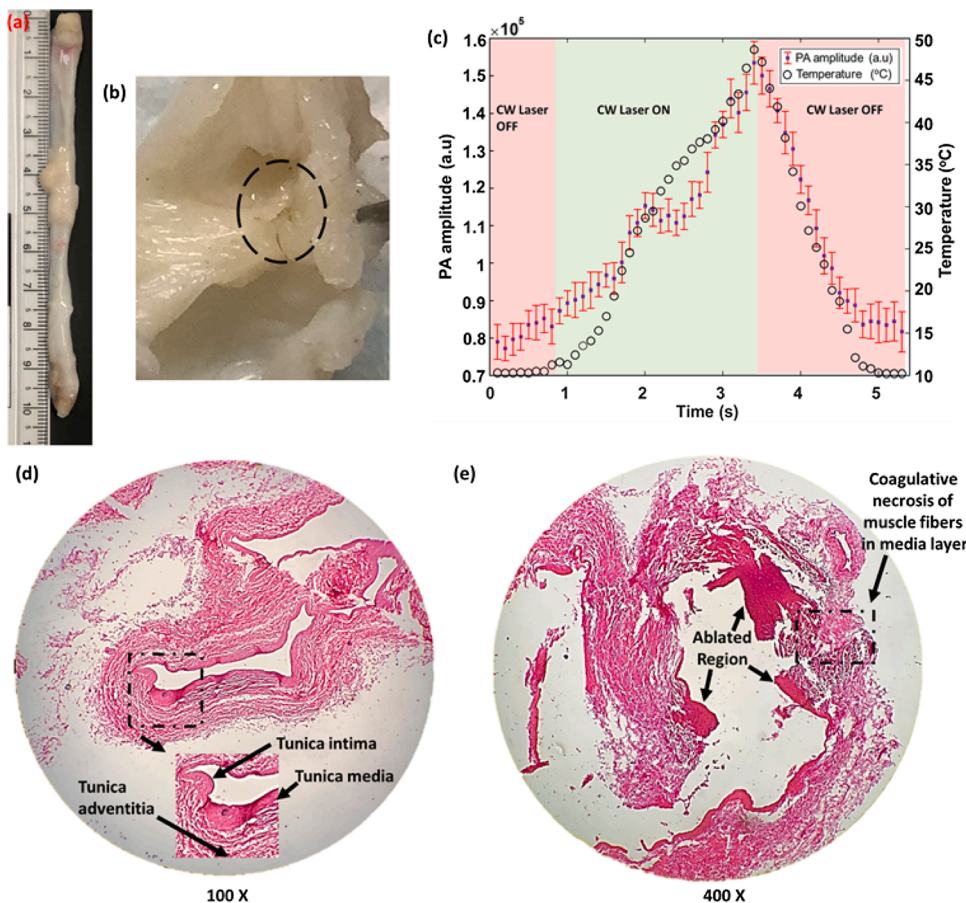

Fig. 4. (a) Photograph of the excised canine jugular vein. (b) Photograph of the thermal lesion formed in the inner wall of the vein (tunica intima). Black dashed circle indicates the ablated area. (c) Changes in the PA amplitude due to temperature changes, when the ablation catheter is placed inside an excised vein tissue. The trough in the graph indicates the drop in the PA amplitude and the formation of the thermal lesion which leads to the closure of the vein. Histology images of the (d) non-ablated (healthy) vein, dashed rectangular region magnified to indicate different layers of the vein and (e) ablated vein, dashed rectangular region indicates the coagulative necrosis of the muscle fibers in the tunica media layer of the vein. Black arrows indicate the damaged regions within the vein.
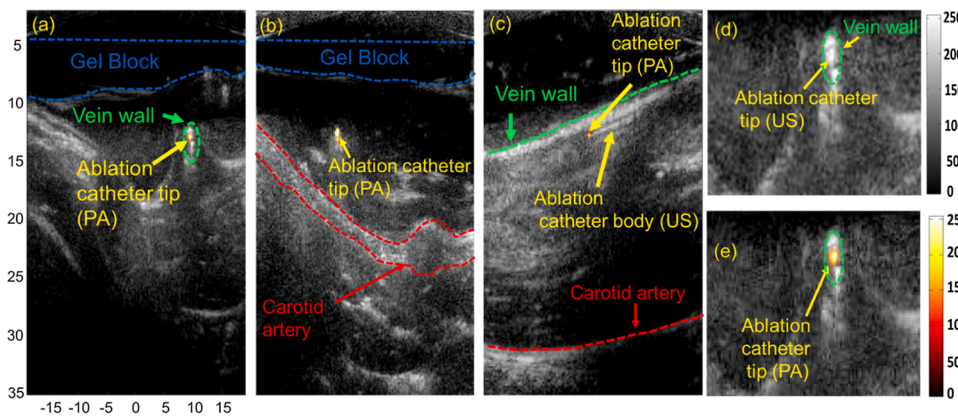
Fig. 5. *In-vivo* USPA imaging for ablation catheter tip tracking during EVLA procedure: (a-b) Transverse and (c) sagittal superimposed USPA images of the ablation catheter tip within the jugular vein. The vein is loosely compressed in (a, c, d, e) and tightly compressed in (b). The anatomical structures of the background tissue are visualized using US imaging. (d) Transverse US image of ablation catheter placed inside the jugular vein. Due to similar US features, US imaging is unable to distinguish between the ablation catheter tip and the vein wall. Transverse USPA image of ablation catheter placed inside the jugular vein. PA detects the ablation catheter tip and US imaging visualizes the background tissue.

3.5. Feasibility of in vivo PA thermometry

The *in vivo* validation study was performed by placing an ablation catheter carrying the combined beam and a temperature sensor inside the jugular vein. The ablation catheter is placed inside the vein in two different scenarios: (a) the ablation catheter is suspended inside the lumen at a suitable distance from the vein wall (Fig. 6a, c), and (b) the tip is placed close to the inner vein wall (tunica intima, water-based tissue) (Fig. 6b, d). The PA amplitude followed the temperature variations caused by the ablation laser but followed a slightly non-linear relationship with an increase in temperature when placed in a blood-filled medium (Fig. 6c). In contrast, the introduction of tumescent anesthesia into the tissues surrounding the vein caused a decrease in temperature (Fig. 6d) and compressed the vein around the ablation catheter (Fig. 6b). During laser ablation, the high absorption of laser energy by the water molecules present in the vein wall at the wavelength of $\lambda = 1470$ nm [6,38] leads to a rapid increase in temperature. As fluence is constant in our study, the increase in the amplitude of the PA signal (Fig. 6d) reflects the temperature-dependent changes in the Grüneisen parameter and the absorption of water molecules present in the vein wall at higher temperatures. This has been validated through our calibration studies (Fig. 6d and e). Hence, the compensated PA curve can quantify the PA signal's dependence on temperature and can be used as a tool for performing quantitative thermometry.

4. Discussion

This report described a novel, integrated PA-guided EVLA system for enhancing EVLA procedures. The developed prototype enhances the capability to track the ablation catheter tip and adds a real-time semi-quantitative temperature monitoring feature to the current US-guided EVLA system. The paper mathematically proved the feasibility of semi-quantitative PA thermometry measurement by compensating the absorption changes of the medium (Section 2-A). Moreover, the *ex vivo* experimental results validate these results by indicating that the PA amplitude generated at the ablation catheter tip is independent of the catheter orientation and the depth at which it is placed (Fig. 2). In addition, we demonstrated that with low energies of 50 μJ, the PA signal was above the detection limit and was able to visualize the catheter tip at tested angular orientations. The absorption compensated results (Fig. 3) for blood and water medium indicates the dependence of the Grüneisen parameter (*i.e.*, the PA signal) with temperature by compensating the temperature-dependent absorption changes. Furthermore, the histology studies (Fig. 4) conducted in the ablated and healthy vein tissues indicated that the integrated system could perform vein ablation. The *in vivo* EVLA tracking experiments explored the tracking and the temperature monitoring capabilities of the integrated PA-guided system. The integrated PA-guided system provides high contrast, background-free, angle-independent images of the ablation catheter tip overlaid with US images of the background tissue. The results (Fig. 5) indicated that the proposed PA images of the ablation catheter tip have a higher SNR twice than the SNR of US images, a CNR nine times higher than the US images. Compared to PA imaging using external illumination, the proposed system utilizes internal illumination, *i.e.*, light coming out of the fiber placed inside the vein, for PA catheter tip tracking and thermometry. Hence, only a small region is illuminated in front of the catheter. Therefore, the PA signals generated arise only from the interface of the catheter tip and the surrounding medium, not from nearby blood vessels. Insensitive to imaging depths, a low-power, high repletion laser can be used for tracking and temperature monitoring capabilities. The PA images have similar SNR and CNR at imaging depths of about 1 cm and 3 cm since the acoustic attenuation of the tissues is relatively low compared to the PA signal amplitude generated at the ablation catheter tip. The integrated PA-guided EVLA system is independent of the imaging depth, catheter orientation and can be translated to DVT treatment procedures using a low center frequency US transducer (bandwidth of 2−4 MHz). The *in vivo* PA thermometry results (Fig. 6) validated the ability of the proposed system to provide precise *in vivo* quantitative PA thermometry estimations.

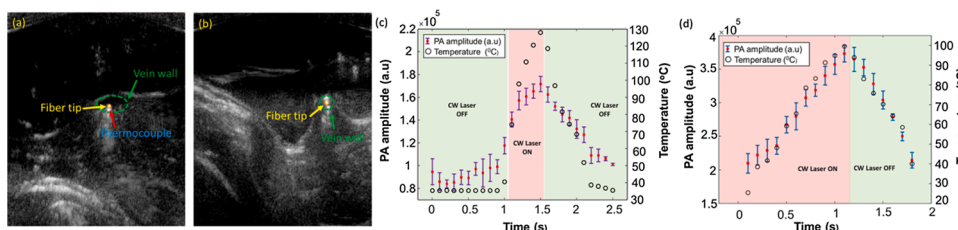The detected PA signal amplitudes in the *ex vivo* study had a high

Fig. 6. PA imaging for real-time thermometry. USPA imaging showing the placement of the ablation catheter and thermocouple (a) suspended in the lumen, placed at a suitable distance away from the vein wall and (b) close to the vein wall. The vein is loosely compressed in (a) and tightly compressed in (b). (c) Changes in PA amplitude due to the temperature changes caused by the CW laser, when the ablation catheter carrying the combined beam is suspended within the lumen and placed (d) close to the vein wall (water-based tissue). Green panels indicate the duration when the CW laser was turned OFF and the red panel indicates the duration when the CW laser was turned ON. The error bars represent the standard deviation along each measurement. (For interpretation of the references to colour in this figure legend, the reader is referred to the web version of this article).

correlation, along with the internal temperature variations. The measured *in vivo* results varied with the *ex vivo* calibration measurements because the temperature of the canine blood was slowly varied. This variation can be accounted for by the rapid increase in temperature caused by the high-power rating of the CW laser within the vein. Our recent studies have indicated that a high repetition rate laser added to the integrated PA-guided EVLA system improves the temporal resolution and monitors rapid temperature variations [40]. Besides, a high repetition laser will provide smoother ablation catheter motions. Since standard EVLA procedures utilize CW laser power levels (3–8 W) for ablation procedures, the variation in the PA amplitude at higher temperatures can be analyzed for providing quantitative temperature measurements for future animal studies. Besides, the blood oxygenation level also plays a vital role in providing quantitative measurements of the ablation catheter tip temperature above 55 °C. During the denaturation of the hemoglobin protein, it gradually loses its combining capability with oxygen. These changes in the oxygenation saturation may increase the variation of quantitative estimation of the ablation catheter tip temperature due to the alterations in the optical and heat properties of the surrounding medium. Using the isosbestic absorption point of oxygen and dioxygen hemoglobin, such as 586 nm, the accuracy of temperature measurements can be improved. When the CW laser stops, there is a rapid decrease in temperature due to the blood flow within the jugular vein, which is usually avoided due to the almost-standstill state of the blood within varicose veins.

The integrated PA-guided EVLA system does not raise any additional concerns to the patient and physician because the average power of the pulsed laser (~1 mW) is approximately four orders of magnitude lower than the CW laser (up to 12 W). This implies that adding a low-power pulsed laser to an existing CW ablation laser poses no risk to the procedure. Moreover, the literature indicates no safety limits for lasers in direct contact with blood vessels [31]. In addition, an identical to the clinically used catheter can be utilized to perform simultaneous PA and ablation. Therefore, no modification measures are required to translate this technology to a clinical setting. The system is easy to adopt, low-cost solution as it does not change the existing EVLA protocol. Current EVLA systems can be easily modified by adding a pulsed laser, dichroic optics, and modifying the imaging sequence to acquire US/ PA images. The *in vivo* studies and easy-to-adopt features have demonstrated that the integrated PA-guided EVLA system can improve EVLA procedures and can be easily translated into the clinic.

5. Conclusion

This study demonstrated the superior capabilities of the PA-guided EVLA system and its clinical stand-by procedures for the treatment of varicose veins in a canine animal model. The integrated system's internal illumination enabled PA imaging provides suitable imaging depths and is not affected by different ablation catheter orientations. The ablation component of the combined beam completely cauterizes and induces a thermal lesion in the vein wall. The histology results indicated permanent obliteration of the tunica intima, tunica externa and indicated vein ablation. The PA thermometry system was calibrated in both blood and water mediums. The *in vivo* canine experiments indicated that PA imaging has high accuracy in tracking the ablation catheter tip and monitoring its temperature in real-time during ablation procedures. The nonlinear variations of the PA amplitude in canine blood with a constant increase in temperature caused due to the changes in the optical properties of blood were studied and validated. Future work will involve evaluating the calibrated PA thermometry in canine models with different CW laser power settings. The accuracy of the calibrated PA thermometry will be further evaluated at the inner vein wall, outer vein wall, and the perivenous tissues through experimental methods and the development of a software-based heat diffusion model.

Appendix A. Supplementary data

Supplementary material related to this article can be found, in the online version, at doi:https://doi.org/10.1016/j.pacs.2021.100298.

References

[1] A. Hamdan, Management of varicose veins and venous insufficiency, Jama 308 (24) (2012) 2612–2621.
[2] R.H. Jones, P.J. Carek, Management of varicose veins, Am. Fam. Physician 78 (11) (2008) 1289–1294.
[3] F. Fowkes, C. Evans, A.J. Lee, Prevalence and risk factors of chronic venous insufficiency, Angiology 52 (1_suppl) (2001) S5–S15.
[4] A. Van Rij, J. Chai, G. Hill, R. Christie, Incidence of deep vein thrombosis after varicose vein surgery, Br. J. Surg. 91 (12) (2004) 1582–1585.
[5] M.S. Weingarten, State-of-the-art treatment of chronic venous disease, Clin. Infect. Dis. (2001) 949–954.
[6] T. Schwarz, E. von Hodenberg, C. Furtwängler, A. Rastan, T. Zeller, F.-J. Neumann, Endovenous laser ablation of varicose veins with the 1470-nm diode laser, J. Vasc. Surg. 51 (6) (2010) 1474–1478.
[7] J.I. Almeida, J.K. Raines, Radiofrequency ablation and laser ablation in the treatment of varicose veins, Ann. Vasc. Surg. 20 (4) (2006) 547–552.
[8] M. Arumugasamy, G. McGreal, C. Kelly, D. Bouchier-Hayes, A. Leahy, The technique of transilluminated powered phlebectomy–a novel, minimally invasive system for varicose vein surgery, Eur. J. Vasc. Endovasc. Surg. 23 (2) (2002) 180–182.
[9] X. Jia, G. Mowatt, J. Burr, K. Cassar, J. Cook, C. Fraser, Systematic review of foam sclerotherapy for varicose veins, Br. J. Surg. 94 (8) (2007) 925–936.
[10] J.I. Almeida, J.J. Javier, E. Mackay, C. Bautista, T.M. Proebstle, First human use of cyanoacrylate adhesive for treatment of saphenous vein incompetence, J. Vasc. Surg. Venous Lymphat. Disord. 1 (2) (2013) 174–180.
[11] W. Malskat, M. Stokbroekx, C. van der Geld, T. Nijsten, R. Van den Bos, Temperature profiles of 980-and 1,470-nm endovenous laser ablation, endovenous radiofrequency ablation and endovenous steam ablation, Lasers Med. Sci. 29 (2) (2014) 423–429.
[12] L. Navarro, R.J. Min, C. Boné, Endovenous laser: a new minimally invasive method of treatment for varicose veins—preliminary observations using an 810 nm diode laser, Dermatol. Surg. 27 (2) (2001) 117–122.
[13] R. Van den Bos, M. Kockaert, H. Neumann, T. Nijsten, Technical review of endovenous laser therapy for varicose veins, Eur. J. Vasc. Endovasc. Surg. 35 (1) (2008) 88–95.
[14] G. Reusz, P. Sarkany, J. Gal, A. Csomos, Needle-related ultrasound artifacts and their importance in anaesthetic practice, Br. J. Anaesth. 112 (5) (2014) 794–802.
[15] M. Ziskin, D. Thickman, N. Goldenberg, M. Lapayowker, J. Becker, The comet tail artifact, J. Ultrasound Med. 1 (1) (1982) 1–7.
[16] S. John, V. Yan, L. Kabbani, N.A. Kennedy, M. Mehrmohammadi, Integration of endovenous laser ablation and photoacoustic imaging systems for enhanced treatment of venous insufficiency, in: 2018 IEEE International Ultrasonics Symposium (IUS), IEEE, 2018, pp. 1–4.
[17] Y. Yan, S. John, M. Ghalehnovi, L. Kabbani, N.A. Kennedy, M. Mehrmohammadi, Photoacoustic imaging for Image-guided endovenous laser ablation procedures, Sci. Rep. 9 (1) (2019) 1–10.

[18] I. Schafhalter-Zoppoth, C.E. McCulloch, A.T. Gray, Ultrasound visibility of needles used for regional nerve block: an in vitro study, Reg. Anesth. Pain Med. 29 (5) (2004) 480–488.

[19] S. John, Y. Yan, S.Y. Forta, L. Kabbani, M. Mehrmohammadi, Integrated ultrasound and photoacoustic imaging for effective endovenous laser ablation: a characterization study, in: 2019 IEEE International Ultrasonics Symposium (IUS), IEEE, 2019, pp. 122–125.

[20] S.A. Braithwaite, B.D. Braithwaite, Clinical utility of the Covidien Closure FastTM endovenous radiofrequency ablation catheter, Med. Devices Auckl. (Auckl) 7 (2014) 179.

[21] R.R. van den Bos, M.A. Kockaert, H.M. Neumann, R.H. Bremmer, T. Nijsten, M. J. van Gemert, Heat conduction from the exceedingly hot fiber tip contributes to the endovenous laser ablation of varicose veins, Lasers Med. Sci. 24 (2) (2009) 247–251.

[22] S.J. Rhee, J. Stoughton, N.L. Cantelmo, Procedural factors influencing the incidence of endovenous heat-induced thrombus (EHIT), J. Vasc. Surg. 53 (2) (2011) 555.

[23] S.J. Rhee, N.L. Cantelmo, M.F. Conrad, J. Stoughton, Factors influencing the incidence of endovenous heat-induced thrombosis (EHIT), J. Vasc. Endovascular Surg. 47 (3) (2013) 207–212.

[24] M. Mehrmohammadi, S. Joon Yoon, D. Yeager, S.Y. Emelianov, Photoacoustic imaging for cancer detection and staging, Curr. Mol. Imaging 2 (1) (2013) 89–105.

[25] P. Beard, Biomedical photoacoustic imaging, Interface Focus 1 (4) (2011) 602–631.

[26] L.V. Wang, S. Hu, Photoacoustic tomography: in vivo imaging from organelles to organs, science 335 (6075) (2012) 1458–1462.

[27] J.L. Su, A.B. Karpiouk, B. Wang, S.Y.J. Emelianov, Photoacoustic imaging of clinical metal needles in tissue, J. Biomed. Opt. 15 (2) (2010) 021309.

[28] C.-W. Wei, et al., Real-time integrated photoacoustic and ultrasound (PAUS) imaging system to guide interventional procedures: ex vivo study, IEEE Trans. Ultrason. Ferroelectr. Freq. Control 62 (2) (2015) 319–328.

[29] D. Piras, C. Grijsen, P. Schutte, W. Steenbergen, S. Manohar, Photoacoustic needle: minimally invasive guidance to biopsy, J. Biomed. Opt. 18 (7) (2013) 070502.

[30] J. Kim, T.T. Mai, J.Y. Kim, J.-J. Min, C. Kim, C.J.S. Lee, Feasibility study of precise balloon catheter tracking and visualization with fast photoacoustic microscopy, Sensors 20 (19) (2020) 5585.

[31] M. Graham, et al., In vivo demonstration of photoacoustic image guidance and robotic visual servoing for cardiac catheter-based interventions, IEEE Trans. Med. Imaging 39 (4) (2019) 1015–1029.

[32] N. Gandhi, M. Allard, S. Kim, P. Kazanzides, M.A.L. Bell, Photoacoustic-based approach to surgical guidance performed with and without a da Vinci robot, J. Biomed. Opt. 22 (12) (2017) 121606.

[33] A.B. Karpiouk, B. Wang, S.Y.J. Emelianov, Development of a catheter for combined intravascular ultrasound and photoacoustic imaging, Rev. Sci. Instrum. 81 (1) (2010) 014901.

[34] F.J.O. Landa, X.L. Deán-Ben, R. Sroka, D.J. Razansky, Volumetric optoacoustic temperature mapping in photothermal therapy, Sci. Rep. 7 (1) (2017) 1–8.

[35] T.F. Fehm, X.L. Deán-Ben, P. Schaur, R. Sroka, D.J. Razansky, Volumetric optoacoustic imaging feedback during endovenous laser therapy–an ex vivo investigation, J. Biophotonics 9 (9) (2016) 934–941.

[36] A.M. Nilsson, G.W. Lucassen, W. Verkruysse, S. Andersson-Engels, M.J. van Gemert, Changes in optical properties of human whole blood in vitro due to slow heating, Photochem. Photobiol. 65 (2) (1997) 366–373.

[37] Q. Peng, et al., Lasers in medicine, Rep. Prog. Phys. 71 (5) (2008) 056701.

[38] F. Pannier, E. Rabe, J. Rits, A. Kadiss, U. Maurins, Endovenous laser ablation of great saphenous veins using a 1470 nm diode laser and the radial fibre–follow-up after six months, Phlebology 26 (1) (2011) 35–39.

[39] D.F. Swinehart, The beer-lambert law, J. Chem. Educ. 39 (7) (1962) 333.

[40] Y. Yan, S. John, J. Meiliute, L. Kabbani, M. Mehrmohammadi, Efficacy of High Temporal Frequency Photoacoustic Guidance of Laser Ablation Procedures, Ultrason. Imaging 43 (3) (2021) 149–156.

Samuel John is a 3rd year Phd student in the Functional and Molecular Ultrasound Research Laboratory at Wayne State University. He is also currently pursuing the dual-title degree in Biomedical Imaging. He has completed his master's in biomedical engineering in Wayne State University and Bachelors in Electronics and Instrumentation Engineering at Sri Ramaswamy Memorial College, India. He has worked on designing rehabilitation and medical robotics, 3D printing, designing microcontrollers, ultrasound and photoacoustic imaging and image-guided procedures. He is the President of the SPIE Student Chapter at Wayne State University. His research is focused on utilizing photoacoustic imaging for enhancing imageguided procedures. He was awarded the SPIE student travel grant award for presenting his research at the SPIE Medical Imaging conference 2018, held at Houston, Texas. He has published the results of hisMaster's thesis in the Scientific Reports Journal, Nature (https://www.nature.com/articles/s41598-018-37588-2). He has also published several IEEE IUS and SPIE conference proceedings related to photoacoustic imaging for image-guided procedures. He has also served as a reviewer for IEEE Access journal (https://publons.com/researcher/3489407/samuel-john/). He has won many hackathons, poster competitions, conducts microcontroller design workshops for students. He has also attended a fully funded research program in China for the development of low-cost brain computer interfaces. He aims to integrate medical robotics and photoacoustic imaging for enhancing image-guided clinical procedures. Research Interest: ultrasound, photoacoustic (PA) imaging, PA thermometry, Image-guided procedures